IOSR Journal of Applied Chemistry (IOSR-JAC)
e-ISSN: 2278-5736.Volume 11, Issue 2 Ver. I (February. 2018), PP 40-54
www.iosrjournals.org

An Insight Into The Interaction of Risedronate Sodium With Human Serum Albumin By Absorption, FT-IR, Fluorescence, SEM, Voltammetry And Molecular Docking Studies

Manjushree M, Hosakere D Revanasiddappa*
Department of Chemistry, University of Mysore, Manasagangothri, Mysuru 570 006, Karnataka, India
**Corresponding Author: Hosakere D. Revanasiddappa (hdrevanasiddappa@yahoo.com)*

Abstract: *Interaction between human serum albumin (HSA) and risedronate sodium (RDT) was investigated by employing (emission and synchronous) fluorescence, ultraviolet–visible (UV-Vis) absorption, Fourier transform infrared (FT-IR) spectroscopic methods, voltammetry, scanning electron microscope (SEM) and molecular docking studies at physiological buffer conditions (pH 7.4). Stern–Volmer and Modified Stern–Volmer equations showed that static quenching, Van't Hoff equation determined the interaction is spontaneous process and the binding is through hydrogen bonds and vander Waals forces. FT-IR reveals that the secondary structure of HSA was altered upon interaction with RDT. UV-Vis, SEM and voltammetric studies were given the information on complex formed between HSA and RDT. The conformation and microenvironment of HSA were changed after the interaction of RDT this was studied by synchronous fluorescence. The calculated binding constant is of the order of 10^5 suggesting that very sTABLE binding. The effects of Fe^{2+}, Cu^{2+} and Zn^{2+} ions were also studied on the binding interaction between HSA and RDT that yields low binding constant values. The binding sites for RDT are present in site III (sub-domain IB) were achieved by ligand displacement and molecular docking studies. This study gives us information on transportation, distribution and toxicity effect of RDT when it enters into human blood serum and it has wide applications in pharmaceutical industry, life sciences and clinical medicine.*

Keywords: *Human serum albumin; Risedronate sodium; Metal ions; Fluorescence spectroscopy; Molecular docking; Binding mechanism*

Date of Submission: 25-01-2018 Date of acceptance: 12-02-2018

I. Introduction

Risedronate sodium, chemically known as [1-hydroxy-2-(3-pyridinyl)ethylidene]bisphosphonic acid] monosodium salt (Fig.1), which is employed mainly for the treatment of integral skeletal disorders like osteoporosis, Paget's disease of bone (osteitis deformans) and also used to strengthen bone. Risedronate sodium is used to suppress osteoclast-mediated bone, inflects bone metabolism and also preventing osteoporosis in postmenopausal women [1-3].

Drug has the important property to bind protein that effects the drug solubility, bioavailability and its half-life in the body. The important protein present in blood plasma is serum albumin involved in drug delivery process into affected tissues in the body. If, binding interaction between serum albumin and drugs is stronger, the availability of free drug is lower; on the other hand, weaker the binding interaction between serum albumin and drugs can lead to a poor distribution of drugs *in vivo*. Therefore, the research on binding interaction between serum albumin with drugs is needful for understanding the action mechanism and pharmacology of drugs [4-7]. High concentration of HSA is present in blood plasma (40 mg/ml or 0.6 mM). This is a globular protein, containing 585 amino acid residues, and it is composed of three structurally similar domains (I, II and III) assemble to form a heart-shaped molecule, each consisting of two sub-domains (A and B) and stabilized by 17 disulfide bridges. Aromatic and heterocyclic ligands usually bind to two hydrophobic pockets in sub-domains IIA and IIIA, called as site I and site II. Seven binding sites are located for fatty acids are sub-domains IB, IIIA, IIIB and on the sub-domain interfaces [8]. They have also high affinity metal binding sites at the N-terminus. HSA has one tryptophan residue Trp-214 that possesses intrinsic fluorescence.

Many metal ions in blood plasma play very important role in biochemical processes. HSA usually acts as a sequestration agent of metal ions and has a variety of metal binding sites with different specificities. The trace elements in biological system may alter the efficacy of the drug; these metal ions are administered along with drug as mineral supplements. The activity of antibiotics, antibacterials, antiviral agents and other drug molecules are affected or sometimes influenced by the interaction of metal ions [9, 10].

These metal ions can form complexes with drug molecules as well as proteins (metal-drug-protein complex), thereby affecting efficacy of the drug. Thus, the distribution, pharmacological properties and metabolism of the drug in blood are affected by this type of interaction.

The chemical literature reveals that no study on the intermolecular interactions of risedronate sodium in the absence and presence of Fe^{2+}, Cu^{2+}, Zn^{2+} ions with human serum albumin. This type of interaction study has prompted us to investigate the binding of drug molecule with HSA in order to understand its efficacy. Hence, in the present work, we used several analytical techniques including emission fluorescence, synchronous fluorescence, ultraviolet–visible (UV-vis) absorption, Fourier transform infrared (FT-IR) spectroscopic, voltammetric, SEM and a computational method (molecular docking studies) at physiological buffer conditions (pH 7.4) to confirm the binding between RDT and HSA. Thus, it is worthwhile to determine the affinity of risedronate sodium to HSA and the efficacy of RDT in presence of metal ions. This study is of great importance in pharmacy, pharmacology and biochemistry.

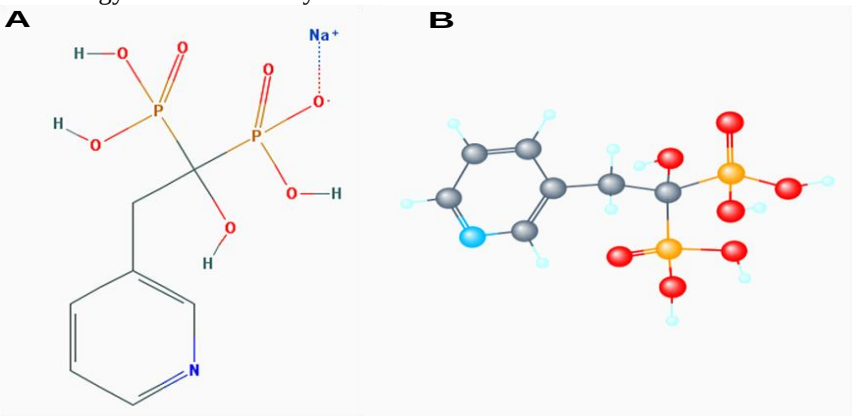

Fig. 1. Molecular (A) and 3D (B) structure of risedronate sodium.

II. Materials and methods

2.1. Reagents

Human serum albumin (HSA; product number: A3782-100MG, lyophilized powder, fatty acid free, globulin free, ≥ 99 %: agarose gel electrophoresis), $(NH_4)_2SO_4.FeSO_4.6H_2O$ (product number: 203505-5G, trace metal basis, 99.997 %), $(CH_3COO)_2Cu.H_2O$ (product number: 326755-25G, 98 %), $ZnSO_4.7H_2O$ (product number: 221376-100G, ACS reagent, 99 %), warfarin (product number: A2250-10G, analytical standard), ibuprofen (product number: I4883-1G, ≥ 98 %: GC) and digitoxin (product number: D5878-250MG, ≥ 92 %: HPLC) were purchased from Sigma-Aldrich (St. Louis, Missouri, USA). Risedronate sodium (RDT; 99.9 %) is received as gift sample from M/S Cipla Ltd, Mumbai and used as such. Doubly distilled water was used to prepare the buffers. The stock solutions of HSA (10^{-4} mol L^{-1}), RDT (10^{-3} mol L^{-1}) and metal solutions of Zn^{2+}, Fe^{2+} and Cu^{2+} (10^{-4} mol L^{-1}) were prepared using Tris-HCl buffer solution (0.05 mol L^{-1} Tris, 0.15 mol L^{-1} NaCl, pH 7.4) and stored in the dark at 4 °C for use.

2.2 Apparatus and procedure

2.2.1. Fluorescence quenching analysis

Fluorescence measurements were performed on a Hitachi Model F-4600 fluorescence spectrophotometer (Tokyo, Japan) equipped with a150W Xenon lamp and an excitation and emission slit width of 10 nm. Excitation wavelength was set at 295 nm and scan mode was emission, using a 1.0 cm quartz cell in the wavelength range of 290–420 nm. The desired temperature was obtained by a circulating water bath and the incubation time for 288 K was 8 minutes in refrigerator and for 308 K 14 minutes in thermostat, this was maintained for all the solutions.

Fluorescence spectroscopy is a powerful analytical tool for the study of chemical and biochemical application with the great sensitivity and specificity. In some cases the difficulty arises for the exact determination of the analyte due to the inner-filter effect. All the fluorescence intensity measurements were corrected for the inner-filter effect using Eq. 1 [11].

$$F_{cor} = F_{obs} \times e^{(A_{ex} + A_{em})/2} \quad (1)$$

where F_{cor} and F_{obs} are the corrected and observed fluorescence intensities, respectively. A_{ex} and A_{em} are the absorbance values of RDT at excitation and emission wavelengths, respectively.

All the fluorescence emission spectra were taken by keeping the concentration of HSA constant (1×10^{-6} mol L^{-1}) while varying concentrations of RDT from 0.0 to 16.0 × 10^{-6} mol L^{-1} [0.0, 1.6, 3.2, 4.8, 6.4, 8.0, 9.6, 11.2, 12.8, 14.4 and 16.0] at different temperatures (288, 298 and 308 K). The blanks should be corrected at

each time from buffer. All of the above solutions were shake well for 5 minutes before being taken their fluorescence spectra.

2.2.2. FTIR spectroscopic measurements

FT-IR spectroscopic measurements were carried out at 298 K on a Spectrum Two FT-IR spectrometer by Perkin Elmer (Waltham, MA 02451 USA) equipped with a germanium attenuated total reflection (ATR) MIRacle Diamond S2PE accessory, a MIRTGS (deuterated-triglycine sulphate) detector and an OptKBr beam splitter. All spectra were taken *via* the ATR method with resolution of 4 cm^{-1} and 60 scans. The FT-IR spectra of HSA (5.0×10^{-6} mol L^{-1}) with risedronate sodium were recorded in the range 1700–1500 cm^{-1} of pH 7.40 Tris-HCl buffer at 298 K. The molar ratio of risedronate sodium to HSA was maintained at 1:1. The absorbance of corresponding contributions of buffer, free risedronate sodium solutions were recorded and subtracted.

2.2.3. Analysis of protein conformation

In globular proteins, the secondary structure is characterized by the shape of the amide I band. Using literature report [12], the spectrum of secondary structure of HSA and its complex with studied drug molecule, the secondary structure of amide I appeared in the region 1700-1600 cm^{-1}. Using Fourier self-deconvolution method, each other in the amide envelope with the help of curve fitting procedure, the area of each peak in amide I of HSA was calculated. By utilizing Origin software the baselines of the spectra were corrected automatically. In the above region, various peaks of HSA and its complex were evaluated. Lorentzian line shape function was used to deconvoluted the spectral region and the deconvoluted peaks were filled by Gaussian band shapes with an iterative curve fitting procedure. The peaks in the region 1615-1637, 1638-1648, 1649-1660, 1660-1680 and 1680-1692 cm^{-1} are corresponding to β-sheet, random coil, α-helix, β-turn and β-antiparallel, respectively [13, 14]. These peaks areas were assimilated and measured by the Gaussian function. The desired conformation was obtained by summing up the area of entire component bands divided by the total area [15, 16]. ORIGINPRO 9.0 32 Bit software was used for curve fitting analysis.

2.2.4. UV–visible absorption measurements

UV-vis absorption spectra were measured on a Beckman Coulter DU 730, Life Science UV/Vis Spectrophotometer (Brea, CA 92821 U.S.A.) equipped with a deuterium (UV) and tungsten (visible) lamps using 10 mm path length quartz cuvettes in the wavelength range of 200–300 nm. Preparations of samples are the same as that of fluorescence samples.

2.2.5. Scanning Electron Microscope (SEM) analysis

The scanning electron microscopic studies were performed using scanning electron microscope with a model S-3400N (Hitachi High – Technologies Corporation – Japan) and all the images were taken at accelerating voltage is 5000 volts, working distance is 4.7 mm and the image resolution is 5µm. SEM images were recorded in solution states at concentrations of HSA = RDT = (HSA+ RDT) = 2×10^{-6} mol L^{-1}.

2.2.6. Voltammetric measurements

Voltammetric measurements were carried out by CHI608E-electrochemical analyser (CH instruments-USA). Working, counter and reference electrodes were Au (gold), a platinum wire and Ag/AgCl electrodes, respectively. Differential pulse voltammograms were obtained by keeping RDT constant (1×10^{-6} mol L^{-1}) and varying concentrations of HSA from 0, 2, 4, 6, 8 and 10×10^{-6} mol L^{-1} at pH 7.4 of Tris-HCl buffer in the potential range from -0.7 to -0.8 V.

2.2.7. Displacement studies

Warfarin, ibuprofen and digitoxin were used as site probes for the competitive ligand displacement for sites I, II and III, respectively. As mentioned in section 2.2.1, different concentrations of RDT and the fixed concentrations of HSA and probe (4×10^{-6} mol L^{-1} each) were used to record emission spectra in order to calculate their (RDT-HSA-probe system) binding constants at 298 K.

2.2.8. Synchronous fluorescence measurements

The excitation and emission monochromator was concurrently scanned for obtaining synchronous fluorescence spectra. The spectra were obtained at concentrations similar to fluorescence quenching studies and employing the setting, $\Delta\lambda = 15$ and 60 nm for tyrosine and tryptophan residues, respectively. The spectra were recorded in the wavelength range of 240–320 nm.

2.2.9. Effects of Fe^{2+}, Cu^{2+} and Zn^{2+} ions

The fluorescence emission spectra of HSA-RDT in the presence of Fe^{2+}, Cu^{2+} and Zn^{2+} ions were taken in the wavelength range of 250-550 nm with the excitation at 280 nm. The concentrations of HSA = 1×10^{-6} mol L^{-1}, metal ions = 50×10^{-6} mol L^{-1} and RDT varies from 0.0, 1.6 to 16.0×10^{-6} mol L^{-1}.

2.2.10. Molecular docking studies

To determine the preferred binding sites on HSA, the docking studies were performed separately for all the three well known sites [Sudlow's sites I (IIA), II (IIIA) and the remaining site named as site III (IB)] by MGL tools 1.5.6 [17] with AutoGrid 4.2.3 and AutoDock 4.2.3 [18] softwares. The X-ray crystal structure of HSA was downloaded from the Protein Data Bank (http://www.rcsb.org/pdb with PDB ID: 1AO6). The structure of HSA was optimized by energy minimization and the lowest energy was obtained using the GROMOS96 43B1 force field parameter set, implemented in Swiss-Pdb Viewer 4.1.0 software. The 3D structure of RDT was generated in Marvin View 5.8.1. During the docking process, water molecules and ions were removed from HSA and the atomic coordinates of chain A of 1AO6 were stored in a separate file and used as input for Auto Dock Tools. Then, polar hydrogens, Kollman charges and solvation parameters were added. For RDT, non-polar hydrogens were merged and rotaTABLE bonds were specified. Lamarckian genetic algorithm was used to calculate the docking calculations with 70 runs and 300 iterations. The binding sites were defined using grid of $60 \times 60 \times 60$ points each with a grid space of 0.375 Å centred at coordinates were x = 32.929, y = 38.860 and z = 36.585 (for site I), x = 16.792, y = 28.194 and z = 20.073 (site II) and x = 44.159, y = 23.089 and z = 18.093 (site III). For each run, a population of 150 individuals by 27,000 generations and 250,000 energy evaluations were performed. And the operator weights for crossover, mutation and elitism were set to 0.8, 0.02 and 1.0, respectively. Cluster analysis was employed on docked results by a root-mean-square deviation (rmsd) tolerance of 2.0 Å. The HSA−RDT complex was visualized and the RDT interactions, binding sites analysed using Biovia Discovery Studio Visualizer v16.1.0.15350.

2.2.11. Statistical Analysis and Curve Plotting

Entire experiments were carried out in triplicate and the obtained results are represented as the mean ± standard deviation (SD). Curve plotting and data interpretations were analysed using Microsoft Excel and OriginPro 9.0 32-bit software (OriginLab Corp., Northampton, MA).

III. Results And Discussion

3.1. Fluorescence spectroscopic studies

3.1.1. Fluorescence emission studies

Fluorescence emission is a well known tool for evaluating the binding of RDT to HSA. Tryptophan, tyrosine and phenylalanine residues are present in HSA causes its fluorescence. Actually, the intrinsic fluorescence of many proteins is mainly contributed by tryptophan alone. This is because of tyrosine undergoes ionization when they are present nearer to carboxyl groups so they are completely quenched and phenylalanine has very low quantum yield [19].

Fig. 2 shows the fluorescence emission spectra of HSA with different concentrations of RDT. Fluorescence intensity of HSA was deliberately decreases with increasing the concentration of RDT, indicating that there was an interaction between HSA and RDT.

Excitation wavelengths for Tyr and Trp were observed at 280 and 295 nm, respectively and their corresponding emission wavelengths at 303 and 335-350 nm [20, 21]. Appropriate in the circumstances, whether Tyr residue is involved in the interaction, HSA fluorescence was excited at 295 nm with different concentrations of RDT, by observing the Fig. 2 there are two emission peaks with a minor blue shift for Tyr from 309 to 307/310 nm and for Trp in range 336 to 334/335 nm. Though the emission peaks for both Tyr and Trp residues were changed but their excitation occurs at 295 nm, this signifies that microenvironment of tryptophan residues altered but not tyrosine. According to these results, the quenching of fluorescence of HSA by RDT is due to tryptophan residue.

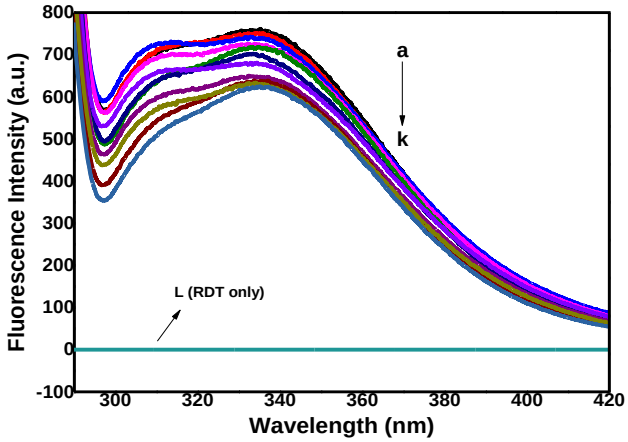

Fig. 2. The fluorescence quenching spectra of HSA by RDT; *c* (HSA) = 1.0 × 10^{-6} mol L^{-1}, *c* (RDT) × 10^{-6} = 0, 1.6 to 16 mol L^{-1} (a to k); curve L represents the emission spectra of RDT only; *c* (RDT) = 20 × 10^{-6} mol L^{-1}; T = 298 K; λ_{ex} = 280 nm; pH = 7.4.

3.1.2. Fluorescence quenching mechanism studies

The various molecular interactions such as excited-state reactions, collision quenching molecular rearrangements, ground-state complex formation, energy transfer etc decrease the fluorescence intensity and this is called as fluorescence quenching process. There are two types of quenching mechanisms namely dynamic and static; they are distinguished by variations in temperature and lifetime analysis. The dynamic quenching occurs when the fluorophore and the quencher approach each other at excited state and static quenching takes place when non-fluorescent complex formation in the ground state. Dynamic quenching process increases with increasing temperature but decreases for static. In order to confirm the quenching mechanism let us assumed that the quenching process may be through dynamic. Hence, for dynamic quenching mechanism Stern–Volmer equation was used [11]:

$$F_0/F = 1 + k_q\tau_0[Q] = 1 + K_{SV}[Q] \quad (2)$$

$$k_q = K_{SV}/\tau_0 \quad (3)$$

where F_0 and F are quencher fluorescence intensities in respectively. k_q, τ_0, K_{SV} and $[Q]$ are the quenching rate constant, average life-time of the biomolecule without quencher (τ_0= 10^{-8} s), the Stern–Volmer dynamic quenching constant and the concentration of the quencher, respectively.

The Stern–Volmer dynamic quenching constants (K_{SV}) were calculated from Stern-Volmer plot F_0/F versus $[Q]$ for the fluorescence quenching of HSA by RDT at different temperatures (Fig. 3A). The calculated K_{SV} and corresponding quenching rate constants k_q are decreases with increasing temperature (TABLE 1). The maximum scatter collision quenching constant (k_q) of verity of quenchers with biopolymer is 2×10^{10} L mol^{-1} s^{-1} [23]. But the accomplished k_q (×10^{12} L mol^{-1} s^{-1}) values are 10.2, 9.5 and 8.4 at 288, 298 and 308 K, respectively. So that quenching mechanism of the binding of RDT to HSA is obtained by the formed complex instead of dynamic collision [11]. At the same time, higher values of K_{SV} might be that the fluorescent quantum yield of HSA increased or there is a strong binding of RDT with HSA. Further, the fluorescence data was determined by using modified Stern–Volmer equation [23]:

$$F_0/(F_0 - F) = (1/f_a) + (1/K_a f_a[Q]) \quad (4)$$

where K_a is the effective static quenching constant for the practicable fluorophores and f_a is the fraction of practicable fluorophore. The plot of $F_0/(F_0 - F)$ *versus* $1/[Q]$, gives $1/f_a$ as the intercept, and $1/K_a f_a$ as the slope. Fig. 3B displays the modified Stern–Volmer plots and the corresponding results of K_a values are tabulated in TABLE 1. The results show that there is a decreasing trend of K_a with increasing temperature. In accordance with K_{SV} dependence on temperature, this coincides with the static type of quenching mechanism. About 68 % of quenching was observed at the highest ligand by protein molar ratio. Hence, this indicates the strong quenching of HSA by RDT.

3.2. The binding constants and the number of binding sites

The binding parameters for the interaction of RDT with HSA were evaluated by fluorescence quenching data. When small molecules bind individually to a set of corresponding sites on a biomacromolecule

referred by static quenching process, the apparent binding constant K_b and number of binding sites n can be calculated by the equation:

$$\log [(F_0 - F)/F] = \log K_b + n \log[Q] \quad (5)$$

where F_0 and F are the fluorescence intensities of fluorophore with and without RDT, respectively and $[Q]$ is the concentration of quencher [24]. Fig. 3C shows the plot of $\log [(F_0 - F)/F]$ *versus* $\log[Q]$ and the obtained values are tabulated in TABLE 1. The obtained K_b values are decreases with increasing temperature because of increase in the diffusion coefficient and a reduction in the stability of the HSA-RDT complex. These results reveal that, strong affinity exists between HSA and RDT. Also, by increasing temperature the ability of RDT to bind to HSA decreases and the binding sites n are approximately equal to 1 indicate that only one RDT molecule bind to HSA.

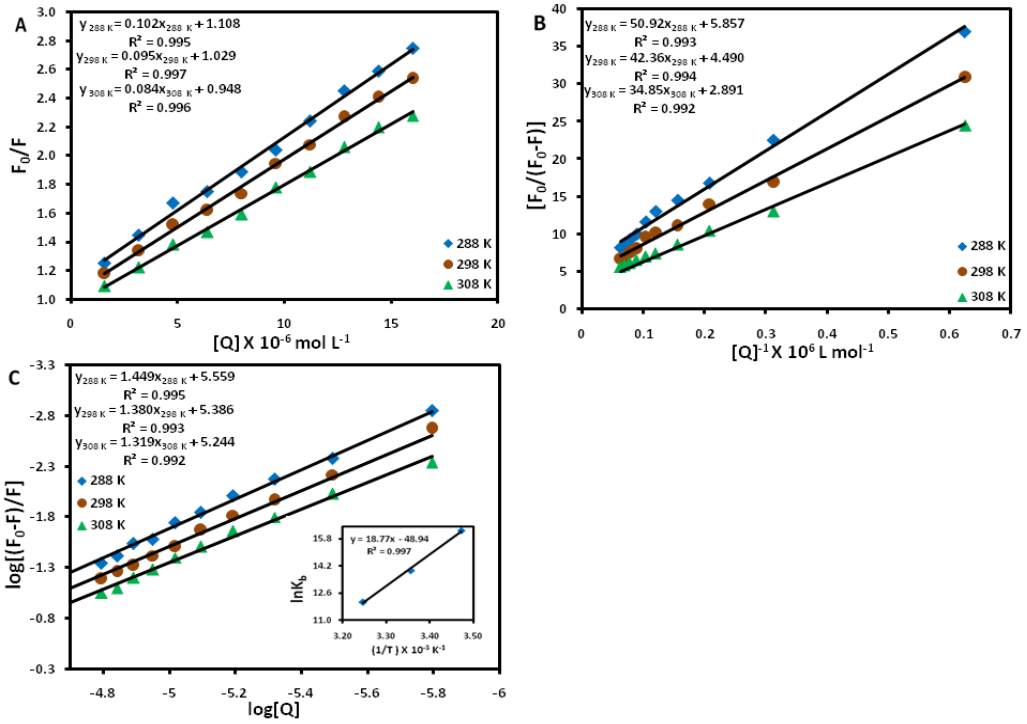

Fig. 3. Stern–Volmer plot (A), Modified Stern–Volmer plot (B), Plot of $\log [(F_0 - F)/F]$ *versus* $\log[Q]$ and (inset C) is van't Hoff plot at different temperatures with pH = 7.4 for HSA-RDT system

TABLE 1

Results of K_{SV}, K_a, K_b and n for HSA-RDT system with different temperatures at pH 7.40

Compound	Temperature (K)	K_{SV} (L mol^{-1}) × 10^4	K_a (L mol^{-1}) × 10^4	K_b (L mol^{-1}) × 10^5	n
HSA-RDT	288	10.2 ± 0.08	11.50 ± 0.02	3.62 ± 0.07	1.449
	298	9.5 ± 0.05	10.59 ± 0.06	2.43 ± 0.01	1.380
	308	8.4 ± 0.10	8.29 ± 0.03	1.75 ± 0.08	1.319

3.3. Thermodynamic parameters and nature of the binding forces

The formation of complex between RDT with HSA is believed to be thermodynamic parameter dependence. Common binding interactions between protein and drug are hydrogen bond, vander Waals force, electrostatic interactions, hydrophobic force, etc. [25]. Van't Hoff equation [26] can be represented as,

$$\ln K_b = (-\Delta H/RT) + (\Delta S/R) \quad (6)$$

$$\Delta G = \Delta H - T\Delta S \quad (7)$$

where ΔH, ΔS and ΔG are change in enthalpy, entropy and free energy, respectively. K_b and R are the binding constant and gas constant, respectively. T is the experimental temperature. According to the van't Hoff relationship, the enthalpy change (ΔH) and entropy change (ΔS) are calculated from the slope and intercept of the plot $\ln K_b$ versus $1/T$ as shown in the inset of Fig. 3C. The free energy change (ΔG) is then estimated using Eq. 7. Thermodynamic parameters are summarized in TABLE 2. From the TABLE, we found that the very low values of ΔG, ΔH and ΔS shows that there is a strong binding interaction between HSA and RDT. The negative values of free energy (ΔG) reveals that the interaction process is spontaneous and the formed HSA-RDT complex is exothermic.

The sign and magnitude of thermodynamic parameters for protein interaction process were obtained by previously reported results they are (i) $\Delta H > 0$ and $\Delta S > 0$, hydrophobic force; (ii) $\Delta H < 0$ and $\Delta S < 0$, vander Waals force and hydrogen bonding; (iii) $\Delta H < 0$ and $\Delta S > 0$, electrostatic interactions. By observing the results

from TABLE 2, ΔH < 0 and ΔS < 0 indicating that the interaction forces between HSA and RDT may be involving vander Waals and hydrogen bonding forces. Since the ΔH value is very low compared to ΔS, so that, the main source of ΔG value was derived from a large contribution of ΔS term with a little contribution from factor ΔH. The negative ΔH and ΔS values for the interaction of HSA and RDT indicates that the binding is mainly entropy driven and enthalpy is unfavorable for it. Thus, it is concluded that the hydrogen bonding has a major role in the interaction, but the weak vander Waals interaction put up a flight.

TABLE 2

Thermodynamic parameters for HSA-RDT system with different temperatures at pH 7.40

Compound	Temperature (K)	ΔG (kJ mol^{-1})	ΔH (kJ mol^{-1})	ΔS (J mol^{-1} K^{-1})
HSA-RDT	288	-38.87	-156.05	-0.406
	298	-34.80		
	308	-30.73		

3.4. FT-IR spectroscopic studies

The interaction between HSA and RDT was further studied by FT-IR spectroscopy. Out of several amide bands, for C=O stretching at 1700–1600 cm^{-1} named by amide I band whereas C–N stretch coupled with N-H bending mode at 1600–1500 cm^{-1} (particularly at 1548 cm^{-1}) termed as amide II band these two amide bands are directly corresponding to changes in secondary structure of HSA [27]. But, different conformations of secondary structure more responsive to amide I band [28-30].

The FT-IR spectrum of risedronate sodium-free form of HSA was obtained by subtracting the absorption spectrum of the buffer solution from the spectrum of the HSA solution (Fig. 4A), the FT-IR spectrum of risedronate sodium-bound form of HSA is obtained by subtracting the absorption spectrum of the RDT and buffer solution (Fig. 4B). The FT-IR difference spectra of free HSA (Fig. 4A) and its risedronate sodium complex (Fig. 4B) in Tris-HCl buffer solution were recorded at 298 K. The peak positions of amides I and II were shifted upon the addition of risedronate sodium to HSA. The shifted peak positions of free HSA/HSA-RDT are tabulated in TABLE 3. The shifted peak positions in FT-IR spectra indicating that the HSA formed a complexes with RDT. The chemical interaction between risedronate sodium and HSA is not a covalent bonding [31-33].

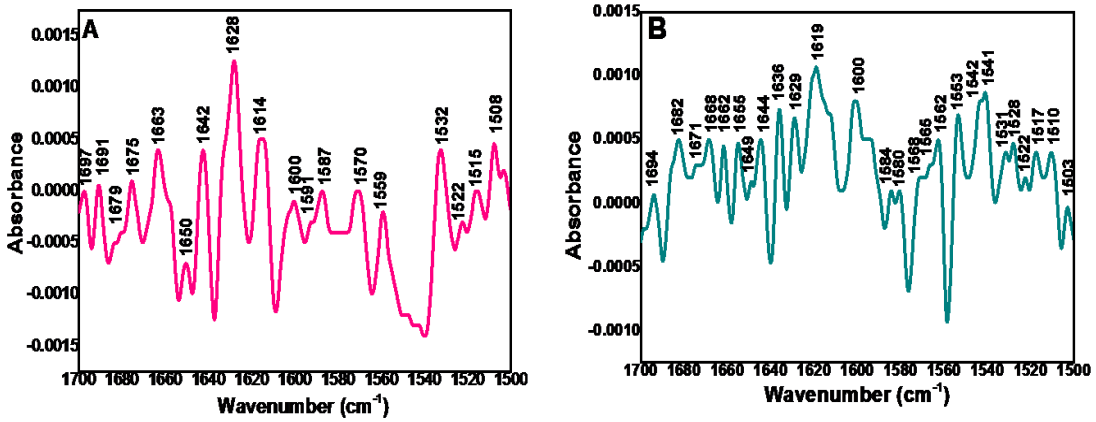

Fig. 4. FT-IR spectra of free HSA obtained by subtracting the spectrum of buffer (A); FT-IR difference spectrum of HSA-RDT bound obtained by subtracting the spectrum of RDT + buffer from that of the HSA-RDT-bound form (B); in the region of 1700-1500 cm^{-1} at physiological pH 7.4 and *c* (HSA = RDT = 5.0 × 10^{-6} mol L^{-1})

TABLE 3

Peak positions in the FT-IR spectra of HSA with RDT at pH=7.4 and T=298 K

Components	Amide I (cm^{-1})					Amide II (cm^{-1})
	1615-1637	1638-1648	1649-1660	1660-1680	1680-1692	1548
Free HSA	1628 ± 0.82	1642 ± 0.67	1650 ± 0.77	1675 ± 0.46	1691 ± 0.53	1532 ± 0.78
HSA-RDT	1629 ± 0.91	1644 ± 0.54	1655 ± 0.81	1668 ± 0.35	1682 ± 0.58	1542 ± 0.26

3.5. Determination of protein secondary structure

Changes in the structure of the protein are reflected by changes in the component band positions of the amide I region [34]. The curve-fitting procedures for infrared self-deconvolution with second derivative were used to determine HSA secondary structures with risedronate sodium. A quantitative analysis of the protein secondary structure for the free HSA with risedronate sodium was carried out, and the results are as shown in Fig. 5 and the percentage of secondary structures of every component is tabulated in TABLE 4. After the interaction of HSA with RDT, there was a major decrease in α-helix and β-antiparallel this is accompanied by

increase in β-sheet, β-turn and random coil. Hence, the change in secondary structures of HSA by RDT indicating that there is an interaction between HSA with RDT.

TABLE 4

Secondary structure analysis by FT-IR spectra of HSA with RDT at pH=7.4 and T=298 K

Components	Secondary structures (%)				
	β-sheet	Random coil	α-helix	β-turn	β-antiparallel
Free HSA	1.58 ± 0.01	24.36 ± 0.08	51.99 ± 0.05	20.72 ± 0.02	1.34 ± 0.07
HSA-RDT	1.70 ± 0.06	19.77 ± 0.02	38.26 ± 0.08	32.10 ± 0.10	8.17 ± 0.06

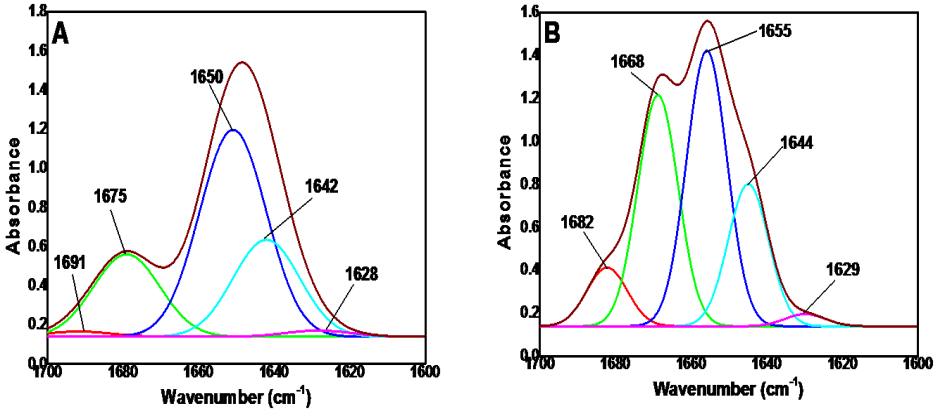

Fig. 5. Second derivative resolution enhancement and curve-fitted amide-I region (1700–1600 cm^{-1}) using Gaussian peak function for free HSA (A); HSA-RDT system (B); *c* (HSA = RDT = 5.0 × 10^{-6} mol L^{-1}) at physiological pH = 7.4

3.6. UV–Vis absorption studies

UV-visible technique is useful to study and confirm the complexation between proteins and drug and also gives the information on structural changes [35]. There are two different peaks that are corresponding to backbone peptide bond and another for aromatic side chain for proteins in absorption spectrum. The nature of electronic transitions are *n* to π* (210-220 nm) and π to π* (190 nm). The intense peaks of back bone amide are found to be at 230 nm, whereas least intense peak at 210 nm for various amino acids. Prominent absorption peaks are occurs at 257, 274 and 280 nm for Phe, Tyr and Trp residues, respectively. Tyr and Trp residues exhibited more intense peaks while a less intense peak for phenylalanine due to π to π* spin-forbidden [36, 37].

Fig. 6 shows the UV-vis absorption spectra of HSA with various concentrations of RDT at pH 7.40. It has been noticed that, the intensity of the absorption peaks increases with increasing concentrations of RDT. It was found that there were two peak positions are at 200-230 nm and 260-280 nm. Again the second peak at 260-280 nm was split into two peaks one showing for Tyr and other one for Trp residues. In addition, a slight red shift differed by 2 nm was observed for both the peak positions. This indicating that the existence of interaction between HSA and RDT and alters the microenvironment of Tyr and Trp residues.

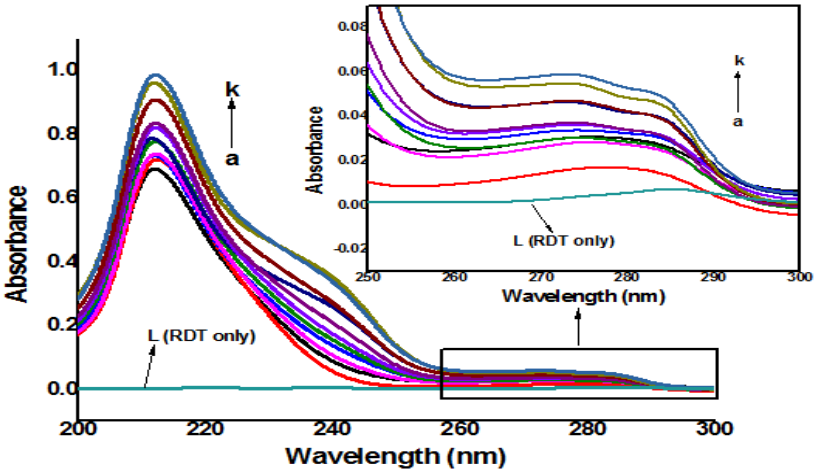

Fig. 6. UV-Vis absorption spectra of HSA-RDT system, curve L shows the UV spectra of RDT only: *c* (RDT) = 20 × 10^{-6} mol L^{-1}, *c* (HSA) = 1.0 × 10^{-6} mol L^{-1} and *c* (RDT) × 10^{-6} = 0,1.6 to 16 mol L^{-1} (a to k); T = 298 K; pH = 7.4.

3.7. Inspection of HSA after interaction with RDT by SEM

The images obtained by SEM for free form of HSA, RDT and their complex (HSA+RDT) are as shown in Fig. 7A, 7B and 7C, respectively. By examining the images, all were unique and having non-identical morphologies. Thus, these images give us information about the formation of complex between HSA and RDT. Hence, this is an additional evidence to understand the interaction between HSA and RDT.

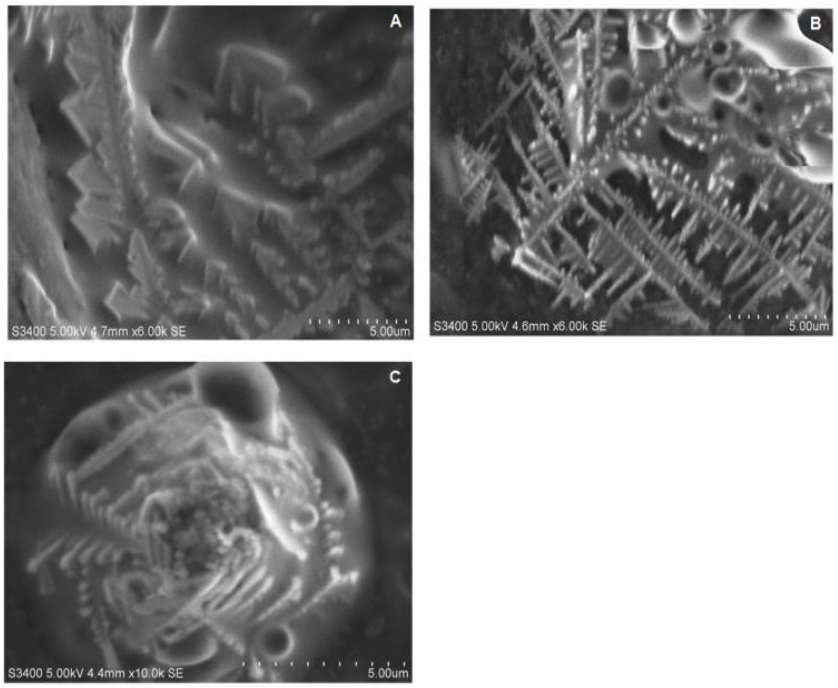

Fig. 7. SEM images for (A) free HSA, (B) RDT and (C) HSA-RDT complex at *c* (HSA) = *c* (RDT) = *c* (HSA+ RDT) = 2×10^{-6} mol L^{-1}

3.8. Voltammetric analysis

In addition to spectroscopic methods, electrochemical techniques were also used for inspecting interactions studies between drugs and proteins, and this can be achieved by observing variations in redox peak current and the shift in potential in voltammogram of RDT in presence of HSA. Fig. 8 shows the differential pulse voltammogram obtained for fixed concentration of RDT with varying concentrations of HSA. It was apparent that addition of different concentrations of HSA to RDT solution decreased the peak current with negative shift in its peak potential of RDT, which has been ascribed to the formation of an eletro-inactive complex. Hence, this result is complement to other experimental data for the existence of interaction between HSA and RDT.

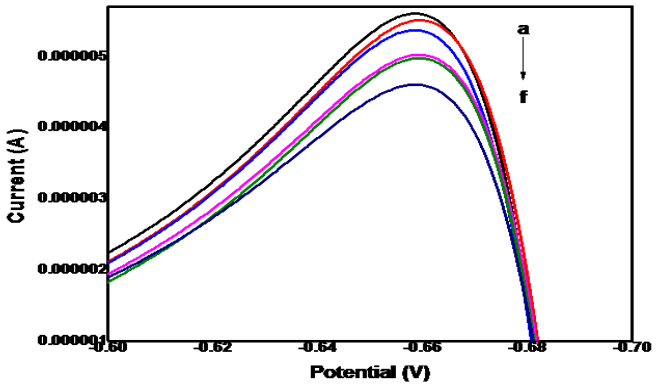

Fig. 8. Differential Pulse voltammograms of HSA-RDT system

3.9. Binding site specificity by site probes for RDT

Ligand displacement experiments were carried out with site-selective probes namely warfarin (site I) and ibuprofen (site II) [38] in order to confirm the specific binding sites between RDT and HSA. In a report [39], the binding between digitoxin and protein is free from Sudlow's sites I and II, and the same interaction was labelled as site III. With the help of fluorescence data (Fig. 9), the binding constants of all the site probes were

calculated using Eq. 5 and the results are given in TABLE 5. The results from TABLE 5 revealed that the binding constant for ibuprofen is not showing any significant changes as compared with K_b value of RDT alone, but the remarkable change was observed for warfarin and digitoxin. The K_b value was decreased largely for digitoxin as compared to warfarin. In conclusion, though Sudlow's site I (IIA) is the binding site for RDT, the most predominant binding site of RDT to HSA is site III based on its very low K_b value (for digitoxin, site III). This result was further confirmed by molecular docking studies.

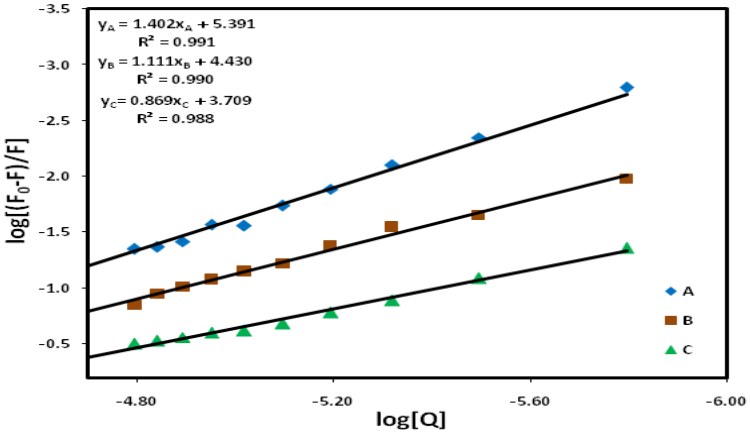

Fig. 9. Plot of log $[(F_0 - F)/F]$ *versus* log$[Q]$. (A) HSA-RDT– Ibuprofen system; (B) HSA-RDT– Warfarin system and (C) HSA–RDT- Digitoxin system

TABLE 5

The comparison of binding constants of RDT-HSA in the absence and presence of site probes at 298 K.

System	K_b (L mol^{-1})
HSA+ RDT	$(2.43 \pm 0.02) \times 10^5$
HSA + RDT + Warfarin	$(2.69 \pm 0.08) \times 10^4$
HSA + RDT + Ibuprofen	$(2.46 \pm 0.01) \times 10^5$
HSA + RDT + Digitoxin	$(5.12 \pm 0.06) \times 10^3$

3.10. Synchronous fluorescence spectroscopic studies

A synchronous fluorescence spectral study gives information about the microenvironment of amino acid residues by using the emission wavelength shift [40]. If the blue shift of λ_{max} occurs, the amino acid residue present highly in hydrophobic environment rather than in solvent, but in the case of red shift, amino acid residues present more in polar environment and more bared to solvent [41].

Fig. 10 shows the synchronous fluorescence spectra of HSA-RDT system. From the Fig. 10 (A) and 10 (A') it has been noticed that, the maximum emission wavelength shift was not observed for tyrosine residue but there was a blue shift of about 2 nm for tryptophan residue shown in Fig. 10 (A'). Therefore, this result shows that the RDT interacting with HSA through tryptophan residues not through tyrosine residues. Thus, the microenvironment of tryptophan residue was altered and it defined more in hydrophobic environment and is less exhibited to solvent. Hence, the polarity around tryptophan residues was decreased and the hydrophobicity was increased.

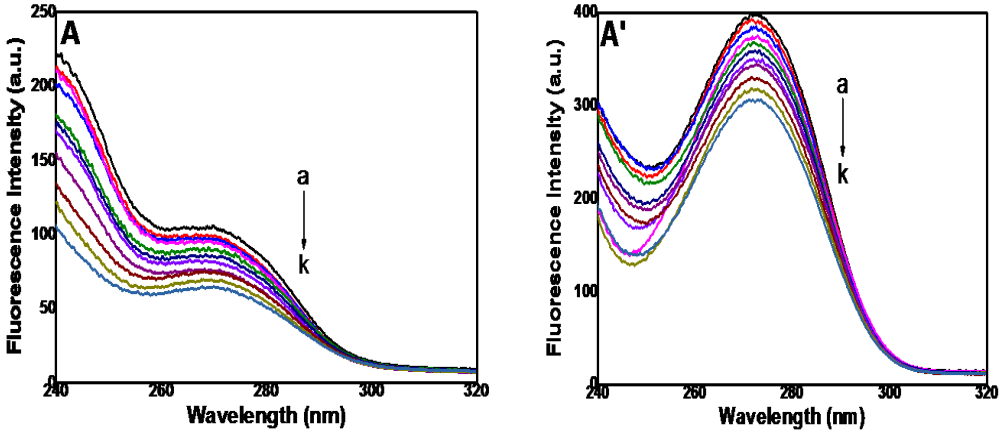

Fig. 10. Synchronous fluorescence spectra of HSA with various concentrations of RDT (A) $\Delta\lambda$= 15 nm; (A') $\Delta\lambda$= 60 nm. The concentrations of HSA and RDT is same as in fig. 3

3.11. Effects of Fe^{2+}, Cu^{2+} and Zn^{2+} ions on the interaction between HSA and RDT

There are many metal ions present in human blood plasma exclusively bivalent states plays a major role in drug-protein binding interaction studies by forming a complex with proteins thereby affecting binding capacity of drugs with proteins [42]. Plot of $\log[(F_0 - F)/F]$ versus $\log[Q]$ for HSA-RDT-Fe^{2+}, HSA-RDT-Cu^{2+} and HSA-RDT-Zn^{2+} systems are as shown in Fig. S1(in the supplementary file). The calculated binding constants for HSA-RDT in the presence of Fe^{2+}, Cu^{2+} and Zn^{2+} ions at 298 K are tabulated in TABLE 6. By observing TABLE 6, reveals that all the three Fe^{2+}, Cu^{2+} and Zn^{2+} ions decreases the binding affinity between HSA-RDT complexes by forming RDT-metal ion complexes. By inferring these results, these three metal ions decreases the availability of free RDT to bind HSA more rapidly, thereby RDT frequently clear from the blood. So that, larger dose of RDT is required to attain the respective therapeutic effects [43].

TABLE 6

Binding constants K_b and number of binding sites n for the systems HSA-RDT with Fe^{2+}, Cu^{2+} and Zn^{2+} ions at 298 K and pH 7.40

compound	K_b (L mol^{-1})	n
HSA-RDT-Fe^{2+}	$(1.91 \pm 0.02) \times 10^3$	0.903 ± 0.005
HSA-RDT-Cu^{2+}	$(1.35 \pm 0.01) \times 10^3$	0.862 ± 0.002
HSA-RDT-Zn^{2+}	$(3.95 \pm 0.04) \times 10^2$	0.714 ± 0.007

3.12. Molecular docking analysis

It is very essential to analyze the binding nature of RDT with HSA for therapeutic and diagnostic facilities. The location of the binding sites in protein can be easily determined by molecular docking study whereas it is quite difficult to understand in experiments conducted at physiological conditions. Molecular docking analysis for Suldow's site I (IIA), Suldow's site II (IIIA) and site III (IB) were conducted separately to predict the RDT preferable binding site on HSA. The evaluated binding modes with different conformations and free binding energies for all the three sites were compared. Binding clusters established for each sites were analysed through root mean square deviation (RMSD) cut-off values. The RDT preferable binding site was decided by largest cluster modes with lowest binding energy. The determined cluster modes (Fig. 11) out of 300 modes for Sudlow's site I (IIA), Sudlow's site II (IIIA) and site III (IB) were 52, 38 and 68, respectively and their corresponding free binding energies were -31.63, -26.19 and -33.15 KJ mol^{-1}. Hence, largest cluster modes with lowest binding energy were obtained for site III (IB). Therefore, site III (IB) is the more favorable binding site for RDT on HSA even though other sites compete. Finally, site III (IB) was further analysed for its binding interactions. All the three sites were separately docked with RDT (Fig. 12). From TABLE 7, it can be noticed that the number of hydrogen bonds and vander Waals interactions were more for site III (IB) compared to other sites. RDT molecule was surrounded by 10 amino acid residues ARG114, LEU115, ARG117, ARG186, MET123, ILE142, VAL116, LEU182, ARG145 and GLU141. Best energy-ranked top 5 results of the binding mode between RDT and HSA for IB based on the binding-site study and values ΔG (binding free energy), $E_{inter-mol}$ (intermolecular interaction energy, which is a sum of vander Waals energy, hydrogen bonding energy, desolvation free energy and electrostatic energy), $E_{vdw+HB+desol}$ (sum of vander Waals energy, hydrogen bonding energy and desolvation free energy) and E_{Elec} (electrostatic energy) are tabulated in TABLE 8. All these results revealed that RDT binding with HSA. Among 10 amino acid residues, four are non-polar (hydrophobic), four are ionic and two are polar. About 50% of the residues belong to the binding pocket are polar and ionic in nature. Also from TABLE 8, $E_{vdw+HB+desol}$ is apparently more negative than E_{Elec} indicating that hydrogen bonding and vander Waals are the major forces in the RDT–HSA complex formation, which is in accordance with the results obtained from theoretically calculated thermodynamics.

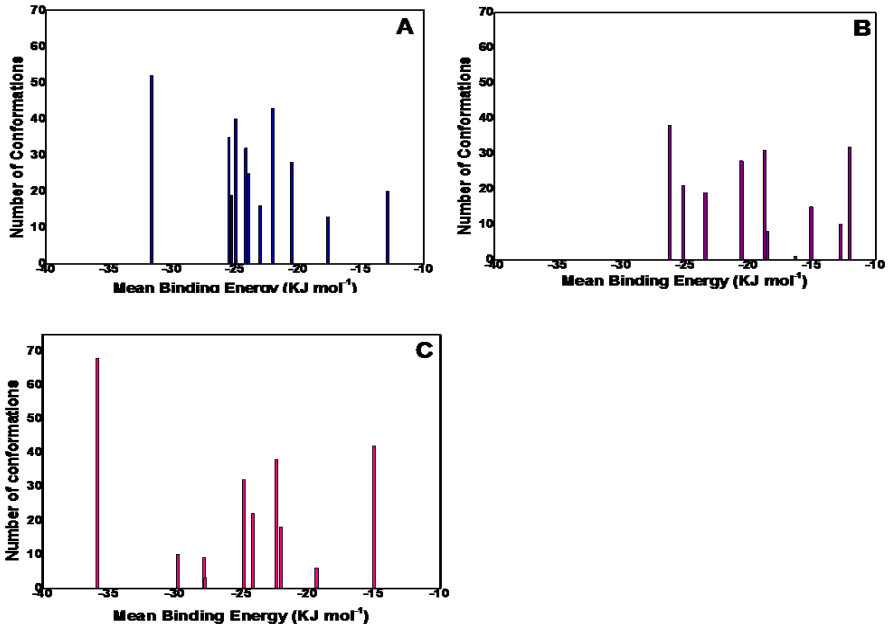

Fig. 11. Docking runs for RDT with HSA showing cluster analysis by AutoDock 4.2.3. Sudlow's site I (A), Sudlow's site II (B) and site III (C)

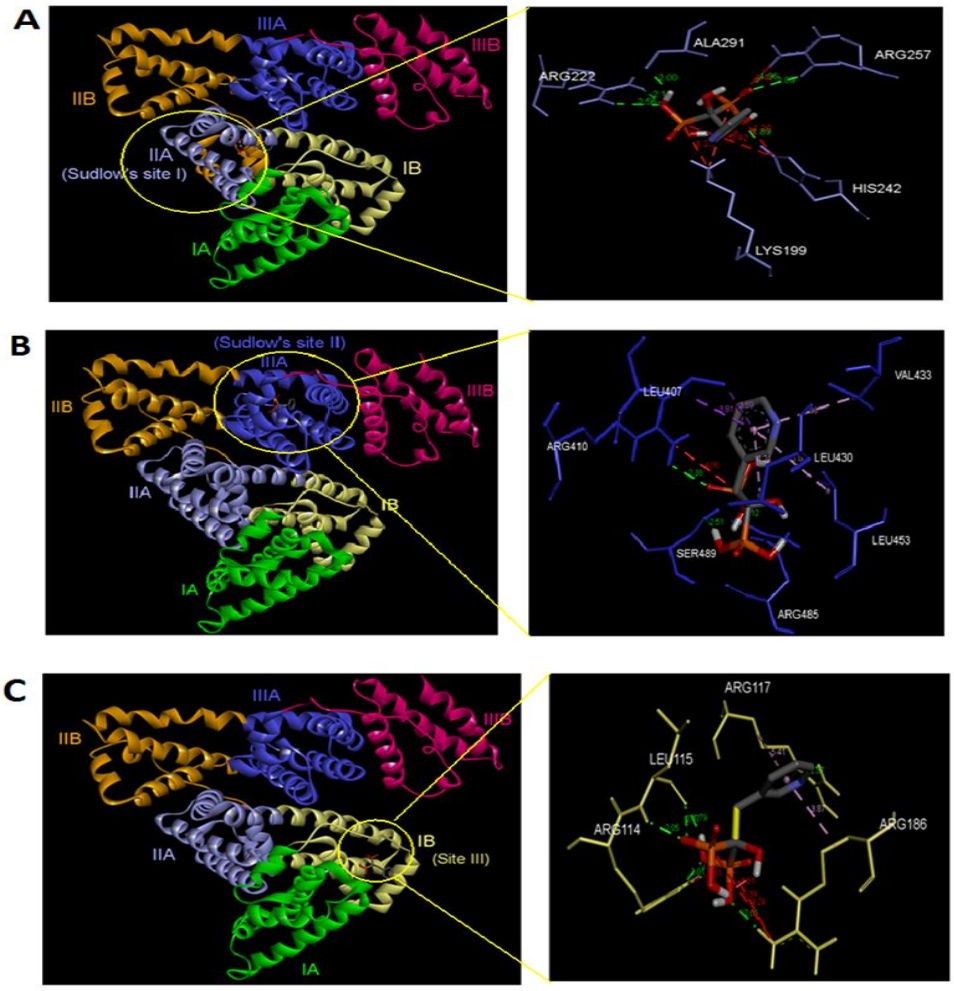

Fig. 12. Molecular docking analysis results by best docking configuration for RDT to HSA: [A] Sudlow's site I (IIA), [B] Sudlow's site II (IIIA) and [C] site III (IB). Each sub-domain is differently colorized and the interactions is separately shown on right side of each [A], [B] and [C]

TABLE 7

Molecular docking analysis for three well known binding sites I, II and III present in HSA with RDT

Binding site	Interactions Type	Distance (Å)	Amino acid – RDT atom
	Conventional Hydrogen Bond	2.56	ARG:222HH21 – O3
		2.00	ALA291:O – H8
		2.89	ARG257:HE – O6
		1.89	HIS242:HE2 – O4
Site I (IIA)	Vander Waals	-	GLU292
		-	TRP214
		-	LEU238
		-	HIS242
	Conventional Hydrogen Bond	2.77	SER489:OG – H7
		2.79	ARG410:HH21 – O7
Site II (IIIA)	Vander Waals	-	LEU457
		-	PHE488
	Conventional Hydrogen Bond	2.05	LEU115:HN – O4
		2.17	LEU115:O – H7
		1.79	LEU115:O – H9
		2.01	ARG114:HE – O2
		2.41	ARG114:HH21 – O2
		2.37	ARG117:HH11 – N1
		2.06	ARG186:HH21 – O3
Site III (IB)		-	MET123
		-	ILE142
		-	LEU115
		-	VAL116
		-	LEU182
		-	ARG145
		-	GLU141

TABLE 8

Docking results of HSA and RDT by using the AutoDock 4.2.3 program generated different ligand conformers using Lamarckian Genetic Algorithm for site III (IB)

Rank	Run	ΔG (KJ mol^{-1})	$E_{inter-mol}$ (KJ mol^{-1})	$E_{vdw+HB+desol}$ (KJ mol^{-1})	E_{Elec} (KJ mol^{-1})
1	68	-33.15	-39.39	-38.84	-0.13
2	57	-32.98	-39.22	-38.71	-0.46
3	3	-32.69	-38.92	-38.30	-0.63
4	30	-28.17	-34.40	-33.90	-0.50
5	61	-27.79	-34.03	-33.98	-0.04

IV. Conclusion

In this work, the interaction between risedronate sodium and human serum albumin were studied by utilizing various spectrometric techniques, voltammetry, SEM and molecular docking studies under physiological conditions (pH 7.4). The results are indexed below:

- As the temperature increases the Stern-Volmer dynamic (K_{SV}) and effective static quenching constant (K_a) were decreases, which indicates that the possible quenching mechanism was static.
- Strong binding between HSA and RDT was revealed by a calculated apparent binding constant (K_b) and number of binding sites (n); these were decreased in presence of metal ions.
- Negative ΔH and ΔS values implies that the vander Waals forces and hydrogen bonding are the major sustaining intermolecular forces for HSA-RDT complex.
- UV-vis, SEM and voltammetric studies given the information on complex formed between HSA and RDT and the conformational changes of amino acids present in HSA.

- The microenvironment changes of Trp residue was investigated from synchronous fluorescence spectra for HSA-RDT system.
- The FT-IR spectra of HSA-RDT complex indicate that the changes in secondary structure of HSA.
- The obtained experimental results are in concordance with the results obtained through molecular docking study and binding site present in site III (IB) was more favorable binding site compared to Sudlow's I and II sites which was further confirmed by ligand displacement experiments.

Various drugs are delivered to particular tissues is mainly by albumins so that the effectiveness of drugs to cure a desirable cause and its adverse effects is easily understood by this study. At the same time, metal ions present in the human body can directly interfere with drug. Hence, this investigation has main attractions in pharmacological studies.

Acknowledgements

The Author Manjushree M thankful to the University Grants Commission, New Delhi for the award of BSR (Basic Scientific Research) fellowship for Meritorious Students, and the Institute of Excellence , University of Mysore, Mysuru for the instrumental facilities.

References

[1]. RxList-The Internet Drug Index, Risedronate, http://www.rxlist.com/cgi/generic/risedronate.html, (accessed 06-04-2017)
[2]. Drug Bank, Risedronate, http://www.pdrhealth.com/drug_info/rxdrugprofiles/drugs/act1580.shtml, (accessed 06-04-2017)
[3]. Drugs.com, Risedronate, http://www.drugs.com/cdi/risedronate-TABLEts.html, (accessed 06-04-2017)
[4]. R.E. Olson, D.D. Christ, Plasma protein binding to drugs, *Annual Reports in Medical Chemistry 31, 1996*, 327-336.
[5]. U. Kragh-Hansen, Structure and ligand binding properties of human serum albumin, *Danish Medical Bulletin, 37(1),* 1990, 57-84.
[6]. U. Kragh-Hansen, V.T.G. Chuang, M. Otagiri, Practical aspects of the ligand-binding and enzymatic properties of human serum albumin, *Biological and Pharmaceutical Bulletin 25(6),* 2002, 695-704.
[7]. B.G. Katzung, S.B. Masters, A.J. Trevor, *Basic & Clinical Pharmacology*, 12th ed., McGraw Hill Lange Publications, US, 2012.
[8]. T. Peters, *All about albumin: biochemistry, genetics, and medical applications*, Academic Press, San Diego, CA, 1996.
[9]. F. Yang, J. Wang, C. Liu, X. Xu, W. Li, Zh. Xia, J. Xiao, Pb^{2+}, Cu^{2+}, Zn^{2+}, Mg^{2+}, and Mn^{2+} reduce the affinities of flavones, genistein and kaempferol for human serum albumin in vitro, *Archieves of Biological Sciences Belgrade 63(3), 2011,* 623–634.
[10]. Nicholas Ferrell, *Transition Metal Complexes as Drugs and Chemotherapeutic Agents*, Kluwer Academic Publishers, The Netherlands, 1989.
[11]. J.R. Lakowicz, *Principles of Fluorescence Spectroscopy*, third ed., Springer-Verlag, Berlin Heidelberg, Berlin/Heidelberg/New York, 2006.
[12]. D.M. Byler, H. Susi, Examination of the secondary structure of proteins by deconvolved FTIR spectra, *Biopolymers 25(3),* 1986, 469–487.
[13]. S.M. Darwish, S.E.A. Sharkh, M.M.A. Teir, S.A. Makharza, M.M. Abu-Hadid, Spectroscopic investigations of pentobarbital interaction with human serum albumin, *Journal of Molecular Structure, 963(2),* 2010, 122–129.
[14]. X.H. Liu, P.X. Xi, F.J. Chen, Z.H. Xu, Z.Z. Zeng, Spectroscopic studies on binding of 1-phenyl-3- (coumarin-6-yl)-sulfonylurea to bovine serum albumin, *Journal of Photochemistry and Photobiology Part B*, 92(2), 2008, 98–102.
[15]. R. Beauchemin, C.N. N'Soukpoe-Kossi, T.J. Thomas, T. Thomas, R. Carpentier, H.A. Tajmir-Riahi, Polyamine analogues bind human serum albumin, *Biomacromolecules 8(10),* 2007, 3177–3183.
[16]. A. Ahmed-Ouameur, H.A. Tajmir-Riahi, R. Carpentier, A quantitative secondary structure analysis of the 33 kDa extrinsic polypeptide of photosystem II by FTIR spectroscopy, *FEBS Letters 363(1),* 1995, 65–68.
[17]. M.F. Sanner, Python: a programming language for software integration and development, *Journal of Molecular Graphics and Modelling, 17(1),* 1999, 57–61.
[18]. D.S. Goodsell, G.M. Morris, A.J. Olson, Automated docking of flexible ligands: applications of AutoDock, *Journal of Molecular Recognition, 9(1),* 1996, 1-5.
[19]. N. Shahabadi, S. Hadidi, F. Feizi, Study on the interaction of antiviral drug 'Tenofovir' with human serum albumin by spectral and molecular modeling methods, *Spectrochimica Acta Part A: Molecular and Biomolecular Spectroscopy,* 138, 2015, 169–175.
[20]. C.R. Cantor, P.R. Schimmel, *Biophysical Chemistry Part II: Techniques for the study of biological structure and function,* W.H. Freeman and Company, New York, 1980.
[21]. Abelson, N. John, Simon, I. Melvin, Brand, Ludwig, Johnson, L. Michael, *Fluorescence Spectroscopy (Methods in Enzymology),* first ed., Academic Press, 1997.
[22]. Y. Ni, S. Wang, S. Kokot, Spectrometric study of the interaction between Alpinetin and bovine serum albumin using chemometrics approaches, *Analytica Chimica Acta, 663,* 2010, 139–146.
[23]. B. Ahmad, S. Parveen, R.H. Khan, Effect of albumin conformation on the binding of ciprofloxacin to human serum albumin: a novel approach directly assigning binding site, *Biomacromolecules 7(4),* 2006, 1350–1356.
[24]. M. Asha Jhonsi, S. Selvaraj, G. Paramaguru, P. Venuvanalingam, R. Renganathan, Spectroscopic and molecular docking investigations on the interaction of rutin with bovine serum albumin, *Zeitschrift Physikalische Chemie. 225(4),* 2011, 441–454.
[25]. P.D. Ross, S. Subramanian, Thermodynamics of protein association reactions: forces contributing to stability, *Biochemistry 20(11),* 1981, 3096-3102.
[26]. M.H. Rahman, T. Maruyama, T. Okada, K.Yamasaki, M. Otagiri, Study of interaction of carprofen and its enantiomers with human serum albumin--I. Mechanism of binding studied by dialysis and spectroscopic methods, *Biochemical Pharmacology 469(10), 1993*, 1721-31.
[27]. J.N. Tian, J.Q. Liu, W.Y. He, Z.D. Hu, X.J. Yao, X.G. Chen, Probing the binding of scutellarin to human serum albumin by circular dichroism, fluorescence spectroscopy, FTIR, and molecular modeling method, *Biomacromolecules, 5(5), 2004,* 1956–1961.
[28]. Y. Li, B. Jia, H. Wang, N. Li, G. Chen, Y. Lin, W. Gao, The interaction of 2-mercaptobenzimidazole with human serum albumin as determined by spectroscopy, atomic force microscopy and molecular modeling, *Colloids and Surfaces B: Biointerfaces, 104,(1)* 2013, 311–317.
[29]. S. Krimm, J. Bandekar, Vibrational spectroscopy and conformation of peptides, polypeptides, and proteins, *Advances in Protien Chemistry 38(1),* 1986, 181–364.

[30]. A.A. Ouameur, S. Diamantoglou, M.R. Sedaghat-Herati, S. Nafisi, R. Carpentier, H.A. Tajmir-Riahi, The effects of drug complexation on the stability and conformation of human serum albumin: protein unfolding, *Cell Biochemistry and Biophysics, 45(2),* 2006, 203–214.
[31]. P. Bourassa, I. Hasni, H.A. Tajmir-Riahi, Folic acid complexes with human and bovine serum albumins, *Food Chemistry, 129(3),* 2011, 1148–1155.
[32]. X.L. Guével, B. Hötzer, G. Jung, K. Hollemeyer, V. Trouillet, M. Schneider, Formation of fluorescent metal (Au, Ag) nanoclusters capped in bovine serum albumin followed by fluorescence and spectroscopy, *Journal of Physical Chemistry A. 115(22),* 2011, 10955–10963.
[33]. Z.G. Peng, K. Hidajat, M.S. Uddin, Adsorption of bovine serum albumin on nanosized magnetic particles, *Journal of Colloid and Interface Science, 271(2),* 2004, 277–283.
[34]. P.M. Bummer, An FT-IR study of the structure of human serum albumin adsorbed to polysulfone, *International Journal of. Pharmaceutics, 132(1*), 1996, 143–151.
[35]. S.Y. Bi, D.Q. Song, Y. Tian, X. Zhou, X. Liu, H.Q. Zhang, Spectroscopic characterization of effective components anthraquinones in Chinese medicinal herbs binding with serum albumins, *Spectrochimica Acta Part A: Molecular and Biomolecular Spectroscopy, 61(1),* 2005, 203-212.
[36]. K.K. Rohatgi-Mukherjee, *Fundamentals of Photochemistry*, Revised ed., Wiley Eastern Ltd, 1986.
[37]. K, Wison, J. Walker, *Practical Biochemistry-Principles and Techniques*, fifth ed., Cambridge University Press, 2004.
[38]. G. Sudlow, D.J. Birkett, D.N. Wade, Further characterization of specific drug binding sites on human serum albumin, *Molular Pharmacology, 12(6),* 1976 1052-1061.
[39]. I. Sjoholm, B. Ekman, A. Kober, I. Ljungstedt-Pahlman, B. Seiving, T. Sjodin, Binding of drugs to human serum albumin: XI. The specificity of three binding sites as studied with albumin immobilized in microparticles, *Molecular Pharmacology, 16(3),* 1979, 767-777.
[40]. W.C Abert, W.M. Gregory, G.S. Allan, The binding interaction of Coomassie blue with proteins. *Analytical Biochemistry 213(2),* 1993, 407–413.
[41]. G. Zhang, Y. Wang, H. Zhang, S. Tang, W. Tao, Human serum albumin interaction with paraquat studied using spectroscopic methods, Pesticide *Biochemistry and Physiology-Journal, 87(3),* 2007, 23–29.
[42]. J. Zhao, X. Jiang, X. Liu, F. Ren, Investigation of effects of temperature and ions on the interaction between ECG and BSA by fluorescence quenching method, *Archives of Biological Sciences, 63(2),* 2011, 325-331.
[43]. P.N. Naik, S.A. Chimatadar, S.T. Nandibewoor, Interaction between a potent corticosteroid drug-examethasone with bovine serum albumin and human serum albumin: A fluorescence quenching and Fourier transformation infrared spectroscopy study, *Journal of Photochemistry and Photobiology B: Biology, 100(3),* 2010, 147-159.

IOSR Journal of Applied Chemistry (IOSR-JAC) is UGC approved Journal with Sl. No. 4031, Journal no. 44190.

Manjushree M. "An Insight Into The Interaction of Risedronate Sodium With Human Serum Albumin By Absorption, FT-IR, Fluorescence, SEM, Voltammetry And Molecular Docking Studies." IOSR Journal of Applied Chemistry (IOSR-JAC) , vol. 11, no. 1, 2018, pp. 40-54.